Chemical Science

ROYAL SOCIETY OF CHEMISTRY

EDGE ARTICLE

View Article Online
View Journal | View Issue

Cite this: *Chem. Sci.*, 2026, **17**, 8726

All publication charges for this article have been paid for by the Royal Society of Chemistry

Two-dimensional Pd–C bonded organometallic framework with dynamic packing transformations

Jong-Yeong Jung, †[a] Jaewook Kim,†[ab] Jintaek Gong,[c] Dongwook Kim,[d] Hee-Seung Lee *[ab] and Hyunjoon Song *[ab]

Traditional metal–organic frameworks (MOFs) are predominantly constructed through metal–oxygen (M–O) or metal–nitrogen (M–N) coordination bonds. However, the limited softness of M–O and M–N bonds restricts the incorporation of softer linkages involving low-valent or noble metals, as described by the hard-soft acid-base (HSAB) principle. Although metal–carbon (M–C) linkages have been proposed as a potential alternative, their limited reversibility and the scarcity of suitable multidentate ligands have hindered their broader implementation in MOF synthesis. In this study, we report the synthesis of a two-dimensional organometallic framework, PdOF-1, which bears direct palladium–carbon (Pd–C) bonds. PdOF-1 was synthesized *via* a one-pot, carboxylate-directed ortho C–H activation process, employing terephthalate (bdc^{2-}) as the organic ligand. The activated carbon atoms of the benzene ring in the bdc^{2-} ligand effectively stabilize the soft palladium centers, yielding an extended network while suppressing palladium agglomeration. Single-crystal X-ray diffraction revealed a zigzag two-dimensional (2D) lattice with ordered layer-by-layer stacking and square-planar Pd coordination. Comprehensive structural and spectroscopic analyses reveal two-step solid-state structural transformations involving layer shearing and compression induced by the removal of intercalated DMSO molecules. In addition, the pristine PdOF-1 undergoes further structural transformation upon solvent exchange with coordinating solvents. This work establishes a new synthetic route bridging organometallic chemistry and reticular design, expanding the chemical space of MOFs toward frameworks with persistent covalent metal–carbon linkages and tunable structural adaptability.

Received 11th November 2025
Accepted 8th March 2026

DOI: 10.1039/d5sc08775a

rsc.li/chemical-science

Introduction

Metal–organic frameworks (MOFs)[1–3] have emerged as a versatile class of crystalline porous materials with a wide range of applications in gas storage,[4] gas separation,[5] catalysis,[6] and energy storage.[7] Their remarkable structural diversity and adaptability arise from the modular assembly of organic ligands and secondary building units (SBUs), whose geometry and connectivity dictate the framework topology. Conventionally, MOFs are constructed *via* coordination bonds between metal centers and oxygen- or nitrogen-based donors, such as carboxylates or azolates, respectively.[8] Accordingly, extensive efforts have been devoted to tailoring ligand geometry and SBU connectivity to achieve new framework topologies and functionalities.[9–12]

Despite these advances, most MOFs remain confined to M–O and M–N linkages, restricting both their electronic tunability and chemical softness. Introducing covalent metal–carbon (M–C) linkages, characteristic of organometallic chemistry, offers a promising path to overcome these limitations, as such bonds provide stronger orbital overlap and enhanced covalency.[13] However, according to the hard-soft acid–base (HSAB) principle, hard carboxylates and intermediate azolates poorly coordinate with low-valent or noble metals, thereby impeding the formation of frameworks incorporating softer linkages (Scheme 1a).[14,15] Moreover, the intrinsic slow ligand exchange kinetics of noble metal ions limit the reversibility of coordination bond formation, posing additional difficulties for the crystallization of uniform frameworks under conventional solvothermal conditions.[16] Consequently, crystalline frameworks with robust M–C bonds are exceedingly rare.[17,18]

To address these challenges, researchers have explored soft donor elements such as carbon and phosphorous to stabilize soft metal centers.[19,20] In particular, organometallic frameworks derived from π-accepting ligands, including isocyanides[21–24]

[a]*Department of Chemistry, Korea Advanced Institute of Science and Technology, 291, Daehak-ro, Yuseong-gu, Daejeon 34141, Republic of Korea. E-mail: hee-seung_lee@kaist.ac.kr; hsong@kaist.ac.kr*

[b]*InnoCORE AI Co-Research & Education for Innovative Drug (AI-CRED) Institute, Korea Advanced Institute of Science and Technology, 291, Daehak-ro, Yuseong-gu, Daejeon 34141, Republic of Korea*

[c]*Department of Chemistry Education, Sunchon National University, 255, Jungang-ro, Suncheon-si, Jeollanam-do 57922, Republic of Korea*

[d]*Center for Catalytic Hydrocarbon Functionalizations, Institute for Basic Science, 291, Daehak-ro, Yuseong-gu, Daejeon 34141, Republic of Korea*

† These authors contributed equally to this work.

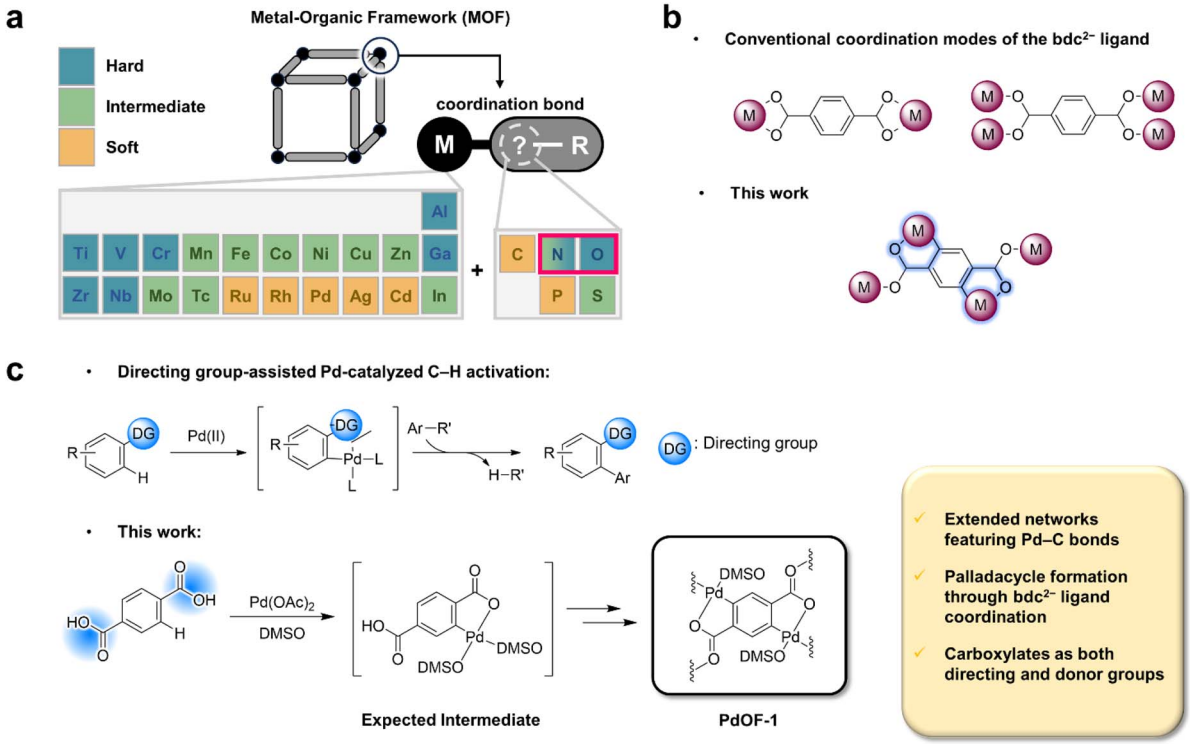

Scheme 1 Rational design strategy for an organometallic framework having Pd–C bonds. (a) Schematic representations of hard-soft trends on metal and ligand elements. (b) Conventional η^2 or η^1 coordination and new metallacycle bonding modes of the bdc^{2-} ligand to the metal centers. (c) Synthetic approach toward PdOF-1 *via* Pd-catalyzed C–H activation directed by carboxylic acids.

and alkynyl groups,[17,18,25] have enabled the incorporation of low-valent metals such as Ni(0), Cu(I), Pd(II), and Ag(I). Yet, these examples depend on pre-functionalized ligands, and their M–C bond formation is often irreversible, limiting both crystallinity and design flexibility. Thus, the development of a robust M–C bonded framework that can be assembled directly from simple precursors remains an unmet challenge at the interface of organometallic and reticular chemistry.

To realize this goal, we revisited a well-established organic linker, terephthalate (bdc^{2-}), widely used in MOF chemistry.[26] While bdc^{2-} typically coordinates through its carboxylate groups to form M–O linkages (Scheme 1b), the carboxylate can also act as a directing group for ortho C–H activation, a key mechanistic step in palladacycle formation. Indeed, Giri and Yu *et al.* reported the first isolated Pd–aryl complex derived from carboxylic acids, as confirmed by X-ray crystallography.[27] More recently, Maiti *et al.* demonstrated the formation of a five-membered palladacycle using pivalic acid and *tert*-butyl acetic acid.[28] These precedents inspired us to translate the concept of carboxylate-directed C–H activation into MOF synthesis, enabling the *in situ* generation of Pd–C bonds within a crystalline framework.

In this study, we present a straightforward and conceptually new synthetic approach for constructing an organometallic framework bearing Pd–C bonds, designated PdOF-1, from Pd(II) and bdc^{2-} ligands (Scheme 1c). Inspired by carboxylate-directed Pd-catalyzed C–H activation in homogeneous systems,[29,30] we exploited the dual functionality of the carboxylate groups in bdc^{2-}: (i) as directing groups that promote regioselective ortho C–H activation, and (ii) as donor sites for subsequent metal–ligand coordination. This dual role enables *in situ* formation of five-membered palladacyclic intermediates featuring covalent Pd–C linkages, which propagate into an extended crystalline framework.

Since such palladacycles are typically intermediates in Pd-catalyzed C–H activation, the solvent plays a crucial role in stabilizing Pd–C species during framework formation. Common solvents typically employed in MOF synthesis, such as alcohols and amides including ethanol and *N*,*N*-dimethylformamide (DMF), are unsuitable because they readily reduce noble metal cations, resulting in Pd(0) particles.[16,31] In contrast, dimethyl sulfoxide (DMSO) suppresses this reduction while weakly coordinating to Pd centers, stabilizing the palladacyclic intermediates.[32] This dual role, confirmed by Pd–S coordination in the crystal structure, enables the formation of PdOF-1, a 2D framework with covalent Pd–C linkages that is chemically and thermally robust under ambient conditions. Furthermore, unlike previous M–C bonded MOFs requiring pre-functionalized ligands,[17,18,21–25] PdOF-1 arises directly from carboxylate-directed C–H activation, bridging organometallic and reticular chemistry.

Results and discussion

PdOF-1 was one-pot synthesized *via* a traditional solvothermal reaction. Among the Pd(II) precursors examined, including

nitrate, chloride, and acetate, only Pd acetate yielded PdOF-1, with the reaction temperature optimized to 80 °C to afford a yield of around 30%. Notably, PdOF-1 have relatively broad temperature window from 80 to 110 °C. Single crystals suitable for single-crystal X-ray diffraction (SC-XRD) were obtained by employing more dilute conditions with excess terephthalic acid and extended reaction times.

The crystal structure of the as-synthesized framework, denoted as PdOF-1(A), was characterized by SC-XRD (Fig. 1). The rigid connection between bdc^{2-} and Pd atoms in PdOF-1 enabled precise structural resolution. PdOF-1(A) consisted of rigid planar repeating units that integrate two square planar metal nodes with a benzene backbone of the terephthalate (bdc^{2-}) ligand (Fig. 1a). These repeating units were connected through coordination bonds at the metal nodes with a torsional rotation along the connecting bond between the adjacent units (Fig. 1b). The assembly of repeating units exhibited a uniform 2D lattice, creating a polymeric sheet structure (Fig. 1c). Due to the non-planar torsional angles ($\Phi_{C-O-Pd-O} = 104°$) between the repeating units, the sheet adopted a zig-zag conformation and stacks in a crest-trough arrangement resembling an AB-stacking mode, with an interlayer spacing of 9.7 Å (Fig. 1d). These stacked layers were further organized in an inclined configuration with a stacking angle of $\beta = 105°$ (Fig. 1e). The interlayer regions formed 2D intersecting channels with a calculated porosity of 42%. DMSO molecules preferentially resided in the region of large interlayer distances within the crest-trough arrangement (Fig. S1a–d), revealing their critical role in stabilizing the AB-stacking mode. In addition, the other DMSO molecules directly coordinated to the Pd metal center contributed to the interlayer stacking by mediating hydrogen interactions between O atoms on one layer and H atoms on an adjacent layer at a distance of 2.670 Å (Fig. S1e and f).

Interestingly, powder X-ray diffraction (PXRD) analysis revealed that PdOF-1(A) undergoes distinct crystal-to-crystal phase transformations upon thermal treatment for 30 min (Fig. 2a and S2). After heating PdOF-1(A) at 70 °C, the characteristic peak at $2\theta = 9.1°$ corresponding to the interlayer spacing of PdOF-1(A) diminished, and new peaks emerged through a crystal-to-crystal transformation (Fig. 2a, black → red). The transformed phase, denoted as PdOF-1(B), was further characterized by SC-XRD (Fig. 2b). The sheets in PdOF-1(B) were arranged in a crest-crest/trough-trough pattern, resembling an AA-stacking mode. This distinct packing structure was more compact than the AB-stacking mode of PdOF-1(A), resulting in reduced porosity and disconnected void spaces with a calculated porosity of 19% (Fig. S3a and b). Consistent with this denser stacking, the interlayer spacing decreased to 7.6 Å,

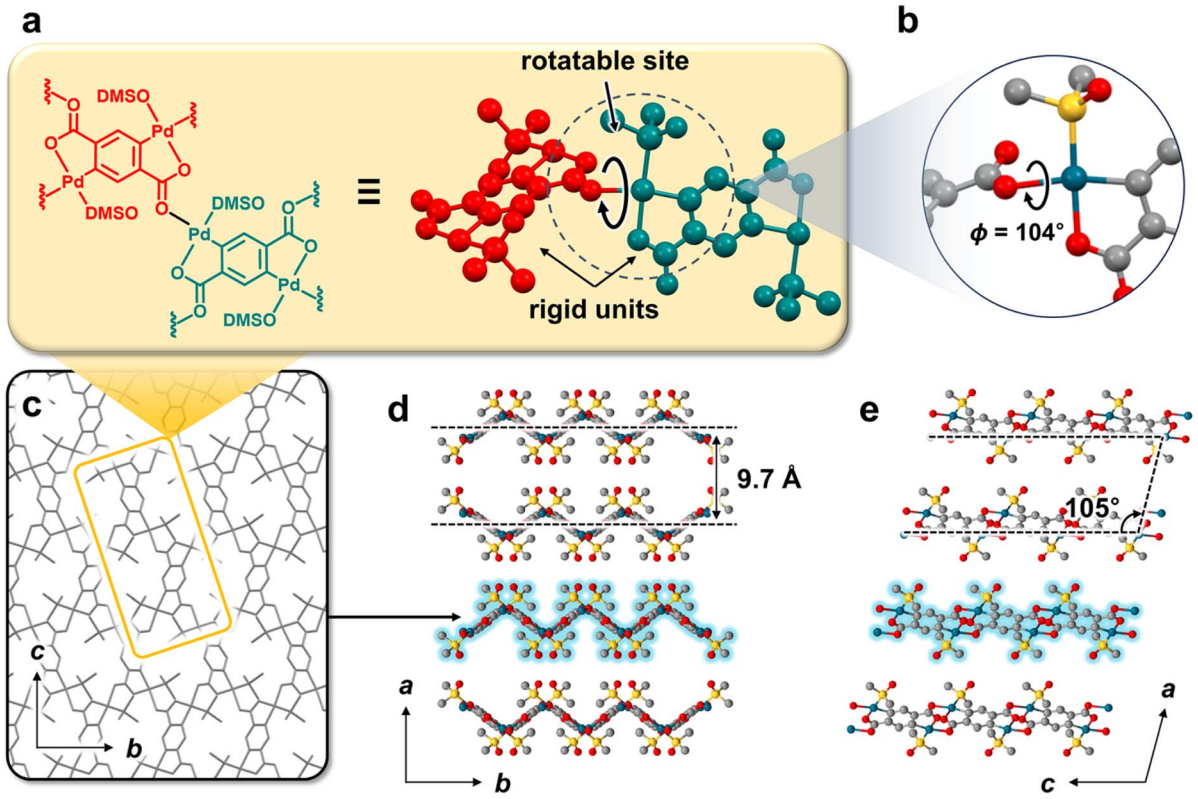

Fig. 1 Structural characteristics of PdOF-1(A). (a) Structural formula (left) and ball-and-stick structure (right) of two repeating units in PdOF-1(A). Each unit is individually colored in red and teal. (b) Highlight of the square planar metal node with a non-planar torsional angle (104°) between the repeating units. (c) A sheet structure formed by assembling the repeating units into a uniform 2D lattice. Crystal structures of PdOF-1(A) along the (d) *c*- and (e) *b*-axis. The layer highlighted in blue represents a single sheet. These layers are stacked with an interlayer spacing of 9.7 Å and an inclined stacking angle of 105°. Pd, C, O, and S atoms are depicted as teal, gray, red, and yellow spheres, respectively. H atoms and intercalated DMSO molecules are excluded for clarity.

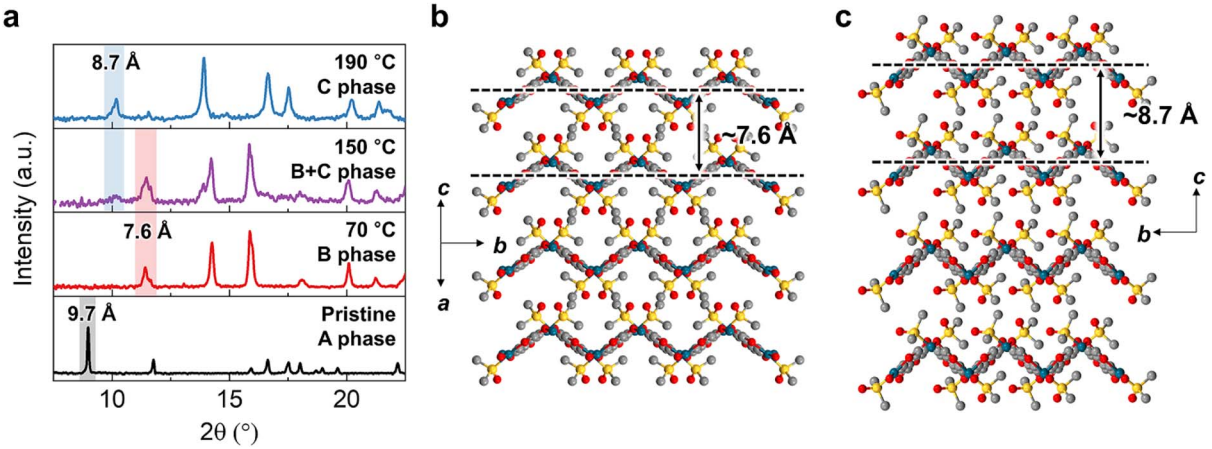

Fig. 2 Structural transformation of PdOF-1 induced by thermal treatment. (a) PXRD patterns of PdOF-1 after heating at various temperatures for 30 min. The characteristic peaks, noted by the colored boxes, indicate the interlayer spacing between sheets of PdOF-1. Crystal structures of (b) PdOF-1(B) and (c) PdOF-1(C) along the front view with their interlayer spacing indicated.

corresponding to the characteristic peak at $2\theta = 11.6°$ in the PXRD pattern. Notably, the DMSO-mediated interlayer hydrogen bonding in PdOF-1(A) persisted after the phase transformation into PdOF-1(B), with a measured distance of 2.790 Å, indicating the crucial role of the DMSO in maintaining the stacking integrity of the framework (Fig. S3c and d).

Further structural transformation was observed by heating PdOF-1(A) from 150 to 190 °C (Fig. 2a, red → blue). As new peaks appeared while those of PdOF-1(B) diminished, a new phase, designated PdOF-1(C), was formed. Due to the crystal fragmentation at high temperatures, the structure solution of PdOF-1(C) by SC-XRD was not feasible. Nevertheless, a plausible structural model for this phase was derived from the Rietveld refinement of the PXRD pattern (Fig. 2c). Compared to PdOF-1(B), PdOF-1(C) exhibited an increased interlayer spacing of 8.7 Å, corresponding to the characteristic peak at $2\theta = 10.2°$ in the PXRD pattern, while simultaneously showing a decrease of porosity to 12%. This inverse trend results from horizontal compression of the 2D layers from 8.0 Å × 15.6 Å to 6.7 Å × 15.5 Å, accompanied by the vertical expansion (Fig. S4 and Table S1). The complete reduction occurred upon heating over 210 °C, forming mostly Pd nanoparticles with a trace amount of Pd_4S (Fig. S2).

The structural analysis of the three PdOF-1 phases reveals that each phase transformation is directly governed by changes in packing arrangement (Fig. S4 and Table S1). During the transition from PdOF-1(A) to PdOF-1(B), the sheet pitch—defined as the crest-to-crest or trough-to-trough distance—remained constant, while the interlayer spacing decreased. The stacking configuration was simultaneously realigned, and the inclined stacking angle increased from 105° to 128°, indicating a shearing motion along the *bc*-plane of PdOF-1(A) with the overall 2D lattice morphology retained. Meanwhile, the phase transformation from PdOF-1(B) to PdOF-1(C) resulted in the intact AA-stacking mode with a uniform inclined stacking angle, indicating negligible shearing. Instead, horizontal compression occurred within the 2D sheets, decreasing the sheet pitch while increasing the interlayer spacing. In a lateral view of a single layer, the bending angles contracted from 106° to 96°, reflecting the horizontal compression (Fig. 3). Nevertheless, the topology of the coordination network in the 2D lattice was insusceptible to compression, and the rigid units based on the square planar coordination of Pd atoms were preserved (Fig. S5), as further supported by spectroscopic analyses (Section S3 and Fig. S6).

Structural transformations in 2D layered frameworks represent an intriguing phenomenon, often driven by modulation of guest or solvent molecules residing between the layers. Variations in the type, amount, or size of intercalated solvent molecules have been shown to induce changes in interlayer distance,[33,34] stacking mode,[35,36] and pore characteristics.[37] Such intercalated solvent-dependent structural adaptability highlights the critical role of intercalated molecules in stabilizing specific layered configurations and enabling phase transformations in 2D frameworks. Motivated by these precedents, we sought to examine in detail how the content of intercalated DMSO governs the phase behavior and structural evolution of PdOF-1.

The structural analysis from X-ray diffraction and thermal analysis revealed that a decrease in DMSO content triggers the rearrangement of the packing structure (Fig. 3, S7, Section S4 and Tables S2–4). The initial step in the thermal gravimetric analysis (TGA) plot for PdOF-1(A) indicates that the evaporation of intercalated DMSO molecules drives the transformation into PdOF-1(B). The reduced porosity and DMSO content in PdOF-1(B) compared to PdOF-1(A) clearly indicate a loss of intercalated DMSO. Further removal of DMSO transformed PdOF-1(B) into PdOF-1(C) with even lower porosity. The scanning electron microscopy-energy dispersive X-ray spectroscopy (SEM-EDS) analyses confirmed the DMSO-to-Pd ratio of 1.60 ± 0.14 in PdOF-1(B) and 0.89 ± 0.02 in PdOF-1(C). The nearly 1 : 1 ratio in PdOF-1(C) confirms that the intercalated DMSO molecules are completely removed during the phase transformation, while the coordinated DMSO molecules are retained.

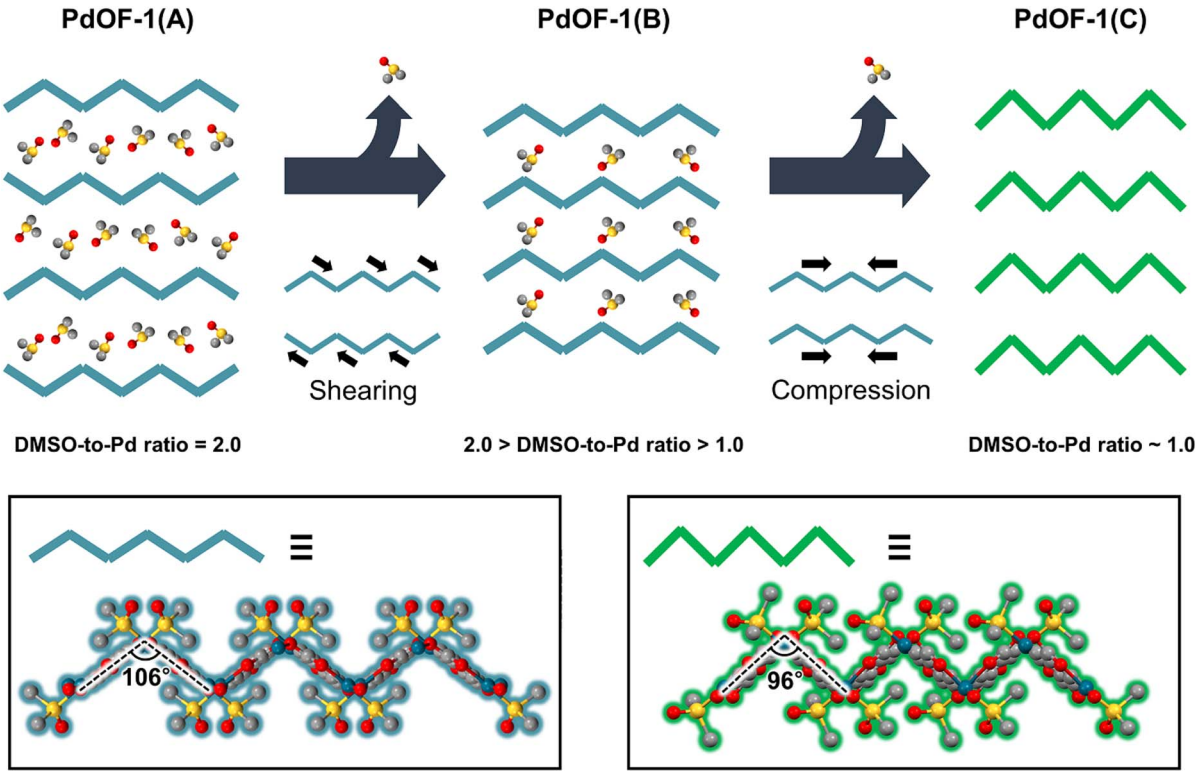

Fig. 3 Proposed mechanism of the structural transformations on PdOF-1. The 2D sheets of PdOF-1(A) and PdOF-1(B) are represented as blue lines, while the compressed 2D sheets of PdOF-1(C) are as green lines. The intercalated DMSO molecules are depicted as ball-stick models between the 2D sheets. The below inset boxes highlight the detailed crystal structure of the cartooned 2D sheets with their bending angles of 106° and 96° for blue and green lines, respectively.

Considering that the DMSO-to-Pd ratio of PdOF-1(B) is approximately 1.6, PdOF-1(B) can be regarded as an intermediate phase between PdOF-1(A) and PdOF-1(C), as the removable intercalated DMSO molecules remain. Nevertheless, PdOF-1(B) exhibits sufficient robustness, as its further transformation into PdOF-1(C) requires higher activation energy to compress 2D layers and remove DMSO completely from all voids. During the transformation of PdOF-1(A) into PdOF-1(B), the DMSO molecules were readily released through the open channels of PdOF-1(A) (Fig. S1a and b). In contrast, the intercalated molecules were firmly trapped in the closed pores of PdOF-1(B), requiring higher energy to be removed entirely (Fig. S3a and b). This confinement of DMSO within the closed framework retards further solvent loss and endows PdOF-1(B) with exceptional structural stability.

Since the depletion of intercalated DMSO drives the transformation from PdOF-1(A) to PdOF-1(B), we further explored solvent-induced structural transformations (Section S5 and Fig. S8). Simple vacuum drying or inert solvent exchanges in PdOF-1(A) also induced the identical phase transformation (Fig. S8a). In addition, the reversibility of the structural transformation between PdOF-1(A) and PdOF-1(B) was investigated by PXRD upon immersion of PdOF-1(B) in DMSO (Fig. S8b). However, phase reversion was not observed, which is attributed to lack of host–guest interaction between DMSO solvents and the frameworks to overcome the energy barrier of restoring PdOF-1(A) phase. While the diffraction peak positions remained unchanged, a marked increase in the intensity of the interlayer reflection suggests enhanced preferred orientation or ordering of the layered structure rather than structural back-transformation.

Interestingly, exchanging with coordinating organic solvents markedly induced different structural changes in PdOF-1(A) (Fig. S8c). Exchanging with thiol solvents generated free H_2bdc ligands and low crystalline phases, indicating degradation of the coordination network in PdOF-1 (Fig. S8c and d). In contrast, pyridine and acetonitrile transformed PdOF-1(A) into new crystalline phases with distinct PXRD patterns while preserving the interactions between Pd atoms and bdc^{2-} ligands. These solvent-dependent structural transformations of PdOF-1 reflects the organometallic and ligand-responsive nature of the Pd centers in PdOF-1, as well as the inherent structural flexibility of the framework itself. Moreover, these features highlight the potential of Pd-based organometallic frameworks as heterogeneous platforms for atomically dispersed Pd centers.

Conclusions

In conclusion, we have successfully synthesized a novel MOF structure incorporating organometallic units with Pd–C bonds generated *via* Pd-catalyzed C–H activation directed by carboxylic

acid groups. By stabilizing soft palladium centers *via* the activated carbon atoms of the bdc^{2-} ligand, our strategy enables the formation of extended frameworks while suppressing palladium agglomeration, providing a general approach for constructing noble metal-based MOFs. The resulting coordination network, composed of palladacyclic Pd–C units, assembles into a uniform zigzag 2D lattice that undergoes packing-selective phase transformations upon modulation of intercalated DMSO content. These phase transformations occur without bond cleavage, demonstrating the intrinsic structural flexibility of PdOF-1. Moreover, the presence of directly coordinated DMSO ligands at the Pd centers suggests promising opportunities for catalysis and the design of responsive functional materials.

Author contributions

The manuscript was written through contributions of all authors. J.-Y. J. conceptualized the synthetic strategy, synthesized the crystals, and managed the experiments. J. K., J. G., D. K., and H.-S. L. solved and refined the crystal structures. J.-Y. J., J. K., H.-S. L., and H. S. analyzed all data and compiled the manuscript. All authors have given approval to the final version of the manuscript. J.-Y. J. and J. K. contributed equally.

Conflicts of interest

There are no conflicts to declare.

Data availability

CCDC 2481799 and 2189180 contain the supplementary crystallographic data for this paper.[38a,b]

The data supporting this article have been included as part of the supplementary information (SI). Supplementary information is available. See DOI: https://doi.org/10.1039/d5sc08775a.

Acknowledgements

The authors acknowledge the Pohang Accelerator Laboratory (PAL) for beamline use. This work was supported by the National Research Foundation (NRF) funded by the Ministry of Science and ICT (MSIT), Republic of Korea (RS-2023-00208239 and RS-2024-00405261), and the InnoCore program of the Ministry of Science and ICT of Korea (N10260004).

Notes and references

1 S. L. James, *Chem. Soc. Rev.*, 2003, **32**, 276–288.
2 H. Furukawa, K. E. Cordova, M. O'Keeffe and O. M. Yaghi, *Science*, 2013, **341**, 1230444.
3 L. Jiao, J. Y. R. Seow, W. S. Skinner, Z. U. Wang and H.-L. Jiang, *Mater. Today*, 2019, **27**, 43–68.
4 R. C. Rohde, K. M. Carsch, M. N. Dods, H. Z. H. Jiang, A. R. McIsaac, R. A. Klein, H. Kwon, S. L. Karstens, Y. Wang, A. J. Huang, J. W. Taylor, Y. Yabuuchi, N. V. Tkachenko, K. R. Meihaus, H. Furukawa, D. R. Yahne, K. E. Engler, K. C. Bustillo, A. M. Minor, J. A. Reimer, M. Head-Gordon, C. M. Brown and J. R. Long, *Science*, 2024, **386**, 814–819.
5 J. Nam, C. Cho, S. Jung, M. Jung, Y. Kim, Y. Hong, S. Lee, H. Oh and W. Choe, *Angew. Chem., Int. Ed.*, 2025, **64**, e202420379.
6 R.-R. Liang, Z. Han, P. Cai, Y. Yang, J. Rushlow, Z. Liu, K.-Y. Wang and H.-C. Zhou, *J. Am. Chem. Soc.*, 2024, **146**, 14174–14181.
7 C. Choi, Y. Luo, A. Reed, G. Whang and B. Dunn, *Chem. Mater.*, 2024, **36**, 11738–11755.
8 S. Yuan, L. Feng, K. Wang, J. Pang, M. Bosch, C. Lollar, Y. Sun, J. Qin, X. Yang, P. Zhang, Q. Wang, L. Zou, Y. Zhang, L. Zhang, Y. Fang, J. Li and H.-C. Zhou, *Adv. Mater.*, 2018, **30**, e1704303.
9 M. J. Kalmutzki, N. Hanikel and O. M. Yaghi, *Sci. Adv.*, 2018, **4**, eaat9180.
10 D. Zhao, D. J. Timmons, D. Yuan and H.-C. Zhou, *Acc. Chem. Res.*, 2011, **44**, 123–133.
11 X.-Y. Dong, Y. Si, J.-S. Yang, C. Zhang, Z. Han, P. Luo, Z.-Y. Wang, S.-Q. Zang and T. C. W. Mak, *Nat. Commun.*, 2020, **11**, 3678.
12 S. M. Moosavi, A. Nandy, K. M. Jablonka, D. Ongari, J. P. Janet, P. G. Boyd, Y. Lee, B. Smit and H. J. Kulik, *Nat. Commun.*, 2020, **11**, 4068.
13 M. Dincă, F. P. Gabbaï and J. R. Long, *Organometallics*, 2019, **38**, 3389–3391.
14 A. M. Hamisu, A. Ariffin and A. C. Wibowo, *Inorg. Chim. Acta*, 2020, **511**, 119801.
15 W.-H. Fang, X. Qi, Y.-L. Xie, J.-Y. Niu, J.-W. Zhao, Y.-M. Li and J. Zhang, *Angew. Chem., Int. Ed.*, 2024, e202417548.
16 T. He, X.-J. Kong, J. Zhou, C. Zhao, K. Wang, X.-Q. Wu, X.-L. Lv, G.-R. Si, J.-R. Li and Z.-R. Nie, *J. Am. Chem. Soc.*, 2021, **143**, 9901–9911.
17 L. Jiang, J. Jia, Y. Ma, Y. Tian, X. Zou and G. Zhu, *Chem*, 2024, **10**, 557–566.
18 L. Jiang, L. Lin, Z. Wang, H. Ai, J. Jia and G. Zhu, *J. Am. Chem. Soc.*, 2024, **146**, 22930–22936.
19 S. G. Dunning, J. E. Reynolds III, K. M. Walsh, D. J. Kristek, V. M. Lynch, P. Kunal and S. M. Humphrey, *Organometallics*, 2019, **38**, 3406–3411.
20 X. Deng, S.-L. Zheng, Y.-H. Zhong, J. Hu, L.-H. Chung and J. He, *Coord. Chem. Rev.*, 2022, **450**, 214235.
21 D. W. Agnew, I. M. DiMucci, A. Arroyave, M. Gembicky, C. E. Moore, S. N. MacMillan, A. L. Rheingold, K. M. Lancaster and J. S. Figueroa, *J. Am. Chem. Soc.*, 2017, **139**, 17257–17260.
22 Y. Dong, J.-J. Jv, X.-W. Wu, J.-L. Kan, T. Lin and Y.-B. Dong, *Chem. Commun.*, 2019, **55**, 14414–14417.
23 K. P. Balto, M. Gembicky, A. L. Rheingold and J. S. Figueroa, *Inorg. Chem.*, 2021, **60**, 12545–12554.
24 K. Jiang, P. Yan, P. Shi, J. Zhang, X. Chai, Y. Wang, C. Zhu, C. Yang, C. Lu, Y. Liu, K. Cao and X. Zhuang, *Angew. Chem., Int. Ed.*, 2025, **64**, e202417658.
25 R. Zhang, T. O'Brien, F. Abdilah, A. J. P. White, P. D. Lickiss and R. P. Davies, *Chem. Commun.*, 2025, **61**, 11637–11640.

26 H. Park, Y. Kang, W. Choe and J. Kim, *J. Chem. Inf. Model.*, 2022, **62**, 1190–1198.
27 R. Giri and J.-Q. Yu, *J. Am. Chem. Soc.*, 2008, **130**, 14082–14083.
28 P. Dolui, J. Das, H. B. Chandrashekar, S. S. Anjana and D. Maiti, *Angew. Chem., Int. Ed.*, 2019, **58**, 13773–13777.
29 T. W. Lyons and M. S. Sanford, *Chem. Rev.*, 2010, **110**, 1147–1169.
30 S. Dutta, T. Bhattacharya, F. J. Geffers, M. Bürger, D. Maiti and D. B. Werz, *Chem. Sci.*, 2022, **13**, 2551–2573.
31 C.-H. Wang, W.-Y. Gao, Q. Ma and D. C. Powers, *Chem. Sci.*, 2019, **10**, 1823–1830.
32 W. Zierkiewicz and T. Privalov, *Organometallics*, 2005, **24**, 6019–6028.
33 X. Li, D. Sensharma, V. I. Nikolayenko, S. Darwish, A. A. Bezrukov, N. Kumar, W. Liu, X.-J. Kong, Z. Zhang and M. J. Zaworotko, *Chem. Mater.*, 2023, **35**, 783–791.
34 H.-M. Zeng, C. Wang, W.-H. Wu, W.-T. Mao, Z.-G. Jiang and C.-H. Zhan, *Nanoscale Adv.*, 2021, **3**, 4680–4684.
35 X. Zheng, H. Liu, J. Cui, Y. Guo, H. Xu, Z. Zhang, J. Zhang and Y. Zhao, *Angew. Chem., Int. Ed.*, 2025, e19150.
36 C. Kang, Z. Zhang, V. Wee, A. K. Usadi, D. C. Calabro, L. S. Braugh, S. Wang, Y. Wang and D. Zhao, *J. Am. Chem. Soc.*, 2020, **142**, 12995–13002.
37 S. Lee, S. Jeong, J. Seong, J. Lim, A. Sharma, S. Won, D. Moon, S. B. Baek and M. S. Lah, *Mater. Chem. Front.*, 2021, **5**, 3621–3627.
38 (*a*) CCDC 2481799: Experimental Crystal Structure Determination, 2026, DOI: 10.5517/ccdc.csd.cc2p9j1l; (*b*) CCDC 2189180: Experimental Crystal Structure Determination, 2026, DOI: 10.5517/ccdc.csd.cc2ch0qm.